Assessing the morphology of selective laser melted NiTi-scaffolds for a three-dimensional quantification of the one-way shape memory effect

Therese Bormann*[a,b], Michael de Wild[b], Felix Beckmann[c] and Bert Müller[a]

[a]Biomaterials Science Center, University of Basel, c/o University Hospital, 4031 Basel, Switzerland;
[b]Institute for Medical and Analytical Technologies, University of Applied Sciences and Arts Northwestern Switzerland, 4032 Muttenz, Switzerland;
[c]Institute of Materials Research, Helmholtz-Zentrum Geesthacht, 21502 Geesthacht, Germany.

ABSTRACT

NiTi is promising for the use as bone scaffold, because the pseudoelasticity or the one- and two-way shape memory effect in the physiological window can mechanically stimulate the adherent cells. Such stimuli can enhance osseo-integration and might reduce stress shielding associated with load bearing implants. The present study is based on the additive manufacturing technique of selective laser melting (SLM) to fabricate three-dimensional NiTi scaffolds. We demonstrate that the morphology of the scaffolds can be quantified using synchrotron radiation-based micro computed tomography (SRμCT) and sophisticated registration software. Comparing the CAD file with the SLM scaffolds, quality factors are derived. With respect to the CAD file, the overlap corresponds to (92.5 ± 0.6) %. (7.4 ± 0.42) % of material was missing and (48.9 ± 2.3) % of excess material found. This means that the actual scaffold is less porous than expected, a fact that has to be considered for the scaffold design. In order to quantify the shape memory effect during the shape recovery process, we acquired radiographs rotating an initially deformed scaffold in angular steps of 0.2 degree during controlled heating. The continuously acquired radiographs were combined to tomography data, showing that the quality factors evolved with temperature as the scaffold height, measured by conventional thermo-mechanical analysis. Furthermore, the data comprise the presence of compressive and tensile local strains in the three-dimensional scaffolds to be compared with the physiological situation.

Keywords: NiTi, scaffold, shape memory effect, selective laser melting (SLM), synchrotron radiation, micro-computed tomography, three-dimensional registration

1. INTRODUCTION

NiTi is a promising candidate for biocompatible load-bearing bone implants as it combines low stiffness with high strength [1, 2]. Near body temperature, it exhibits characteristic properties including pseudoelasticity, the one-way shape memory effect and high damping capacities caused by a reversible crystalline transformation between the austenite and martensite crystalline phase, which are another advantage for osseo-integration of load-bearing implants [2]. The mechanical stimulation of the bony tissues enhances re-modeling and therefore the osseo-inductive behavior [3, 4]. Selective laser melting is a versatile method to prepare porous scaffolds with a variety of regularly arranged unit cells. These open porous structures are generated using computer aided design (CAD). The designs are materialized applying appropriate precursor powders and suitable laser parameters. The selection of powder and laser parameters enables the operator to tailor the structural and thermal properties of the porous constructs [5, 6].

In a porous system including scaffolds or textiles both tensile and compressive strain simultaneously occur even only compression or tensile load is applied (see Fig. 1). Human cells such as osteoblasts might therefore behave in different fashion depending on their location within the scaffold and might migrate toward the preferred location within the unit cell of the scaffold.

Local strains occurring in a porous NiTi scaffold during shape changes induced by heating should be quantified and visualized taking advantage of synchrotron-based micro computed tomography (SRμCT) and sophisticated software tools for rigid and non-rigid registration [7].

*therese.bormann@unibas.ch; phone +41 61 26 59 127, //www.bmc.unibas.ch

Behavior and Mechanics of Multifunctional Materials and Composites 2013, edited by Nakhiah C. Goulbourne, Hani E. Naguib, Proc. of SPIE Vol. 8689, 868914
 · doi: 10.1117/12.2012245

These spatially resolved strains could in a next step be directly compared with strains acting on cells in a physiological environment such as the human body. In bones for example, values for strains induced by normal activity lie between 0.005 % and 0.5 % [8, 9]. The application of such micro-strains during in-growth of implants has shown to increase parameters like bone-to-implant contact [10, 11].

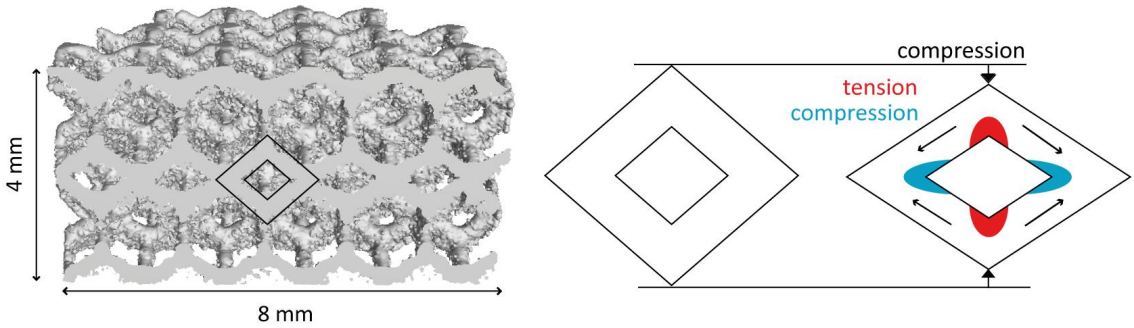

Fig. 1. Three-dimensional rendering of µCT data of a transversally cut NiTi scaffold. The cross section of the unit cells is approximated as diamond shape as indicated. The scheme illustrates the expected local tensile and compressive strains in a unit cell under compression.

We hypothesize that the local strains, which are generated by defined compression of porous NiTi scaffolds prepared by selective laser melting correspond to actual strains occurring in a physiological situation. Cells within the scaffolds should therefore show specific reactions depending on their location and NiTi scaffolds might prove to be clinically relevant for future medical applications.

As a first approach, we are presenting a SRµCT setup to continuously investigate pseudoplastic NiTi scaffolds during their shape recovery process. The method is validated by extracting quantities describing the scaffolds morphology during the heating period and comparing the evolution of these quantities with temperature to conventional thermo-mechanical analysis (TMA) measurements. Furthermore, the scaffolds morphology and deviations from the initial CAD design can be assessed locally and globally by the presented method.

2. MATERIALS AND METHODS

2.1 Scaffold preparation

Selective laser melting (SLM Realizer 100, Realizer, Borchen, Germany) served for the fabrication of scaffolds with sub-millimeter precision from pre-alloyed NiTi powder with a nominal Ni-content of 55.96 wt.-% (Memry GmbH, Weil am Rhein, Germany). The outer dimensions of the scaffolds referred to 8 mm in diameter and 4 mm in height, respectively. The scaffold geometry is defined in a CAD model based on a rhombo-dodecahedral unit cell of $(2\ \text{mm})^3$ with 300 µm thin struts. Subsequent to fabrication, the specimens were subjected to annealing under Ar atmosphere at a temperature of 500 °C for a duration of 25 minutes, which was followed by furnace cooling. The resulting phase transformation temperatures were determined by differential scanning calorimetry (DSC 30, Mettler-Toledo) at a heating rate of 10 K per minute. The austenite start temperature (A_s) corresponded to 25 °C, the austenite peak temperature (A_p) to 35 °C and the austenite finish temperature (A_f) to 41 °C.

For the investigation of the shape recovery process by synchrotron radiation-based micro computed tomography (SRµCT), a scaffold with an original height of 4.01 mm was pseudoplastically deformed by compression along its *z*-axis by 260 µm prior to the SRµCT experiment. To ensure a fully martensitic crystalline structure during deformation, the specimen was cooled down in liquid nitrogen before deformation.

Thermo-mechanical analysis (TMA) of a scaffold, pseudoplastically deformed by compression along its *z*-axis about 265 µm, was done by the TMA 40 (Mettler-Toledo) at a heating rate of 0.083 K per minute in a temperature range from 18 °C to 35 °C.

2.2 Synchrotron radiation-based micro computed tomography setup

SRµCT investigations were carried out on scaffolds prior to deformation, during the shape recovery process induced by controlled heating and subsequent to deformation. The beamline W2 (DESY, Hamburg, Germany) operated by the

Helmholtz-Zentrum Geesthacht served for the tomography data acquisition in the conventional absorption contrast mode [12]. The photon energy was set to 70 keV and projections on a field of 3056*3056 pixels with an effective pixel size of 3.2 µm were recorded in angular steps of 0.2 degrees. Because of the parallel X-rays, the radiographs of the scaffold in original and deformed states were acquired from a 180° rotation. The spatial resolution determined from the modulation transfer function of a highly X-ray absorbing edge [13] corresponded to 7.2 µm.

To investigate the specimen during the one-way shape memory effect, radiographs of the initially deformed scaffold were recorded constantly while the scaffold was subjected to heating. During the heating period 4853 radiographs were obtained, which corresponds to a sample rotation of 970.6 degrees. Heating of the specimen was carried out in a water bath with a rate of 0.067 K per minute, whereas the starting temperature corresponded to 15 °C and the experiment was terminated at a temperature of 37 °C. These thermo-electrically measured temperature values were downwards corrected by about 7.5 K based on a temperature calibration using the TMA measurement of a deformed scaffold from the same processing batch.

2.3 Tomographic reconstruction

Before reconstruction, the recorded radiographs were two-fold binned to improve the photon statistics [14]. The reconstruction was performed by means of the filtered back-projection algorithm [15]. Eleven three-dimensional datasets were reconstructed over the heating period using the 4853 projections in total. The starting angle for each subsequent reconstruction was increased by about 79°. Each of the reconstructed datasets covered a temperature interval of 3 to 5 K. To reduce data size, the datasets were binned after reconstruction for a second time by a factor of two leading to an effective pixel size of 12.93 µm in the datasets used for the 3D registration [16].

2.4 Data treatment

To assess the morphological quality factor of the SLM-fabricated scaffold with regard to the CAD model and to quantify the differences caused by deformation and shape recovery, the tomography datasets were rigidly registered with the CAD design. Rigid registration means, that six independent parameters, three for translation and three for rotation, have to be found.

As the used registration algorithm [17] works on voxel-based three-dimensional data, the CAD data was converted prior to registration, since SLM, as most additive manufacturing methods, is based on a surface triangulated file format (.stl). The CAD file in .stl-format was thus converted into a voxel-based .raw data format using Matlab (2010b, The MathWorks, Natick, USA) code. The voxel size of the dataset was set to $(13\ \mu m)^3$ according to the reconstructed tomography data. The voxel size was further refined to 12.82*12.82*12.99 µm³ to reduce differences between the .stl and .raw-file. All further data processing was done using the Matlab code. For data visualisation, however, we applied VG Studio Max 2.1 (Volume Graphics, Heidelberg, Germany).

2.5 Volume-based segmentation

The reconstructed datasets showed artefacts like blurring and periodic variations in the local absorption values, which were caused by the deformation of the scaffold during the shape recovery. The presence of these artefacts increased the visible strut thickness in the reconstructed data and the background in the histograms of the local X-ray absorption coefficients. The identification of a reasonable threshold for the scaffold segmentation was therefore not straightforward. As the mass of the NiTi scaffolds is known and as we can consider the density and volume to be constant during the measurements, we can reasonably follow a volume-based approach.

As the literature values for the density of NiTi vary between 6.40 and 6.51 g/cm^3, we measured the density of the starting material (prior to atomization) by Archimedes principle with a tensiometer (K11, Krüss, Hamburg, Germany), which returned a value of $(6.52 \pm 0.02)\ g/cm^3$. Based on the specimen weight of 0.3 g, the scaffold volume corresponds to $(46.0 \pm 0.7)\ mm^3$. Segmentation between material and background was than accomplished by choosing the threshold such that the volume of the segmented data matched the specimens calculated volume.

3. RESULTS AND DISCUSSION

3.1 Quality assessment via 3D registration

To assess the overall quality of the SLM fabricated scaffold, the SRµCT dataset of the non-deformed scaffold was rigidly registered with the 3D dataset of the design (CAD model). Figure 2 displays the .stl-file of the CAD model (A),

the SLM-built NiTi scaffold (B) prior to deformation and an overlay of the .stl-file and the scaffold after registration (C, D). From first glance, the lattice shape was matched well by the SLM scaffold. Nevertheless, the main difference of the SLM specimen in comparison to the initial file is protruding material along the struts, as visible from the images in Figure 2 (C) and (D).

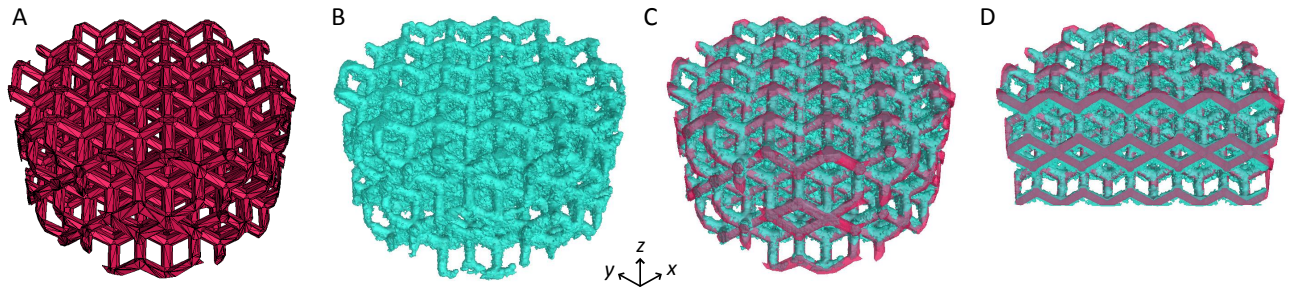

Figure 2. 3D rendering of the CAD .stl-file (A), the SRμCT scan of the non-deformed scaffold (B), overlay of the CAD file and the scaffold after registration (C), and a virtual cut through the latter (D). Diameter of the scaffold refers to 8 mm, height to 4 mm.

To quantify the morphological quality of the SLM built scaffold, we subtracted the registered SRμCT dataset from the CAD file and analyzed the resulting three-dimensional matrix regarding protruding, deficient and overlapping material in reference to the matrix of the initial CAD file [18]. For the whole scaffold, we found that (92.55 ± 0.55) % of the initial matrix overlaps with the SLM scaffold, (48.87 ± 2.30) % is protruding the initial matrix and (7.45 ± 0.42) % of the targeted volume is missing. This means that the actual scaffold is less porous than designed. The intended relative open pore volume corresponded to 84 %, whereas we find in the actual scaffold an open pore volume of about 76 %. With other words, one has to consider this phenomenon in the scaffold design.

To gain closer insight into the material distribution within the scaffold, we analyzed the difference in the registered datasets by the local determination of excess, missing or overlapping material for each slice of voxels along the *x*-, *y*- and *z*-axis, respectively. The results are displayed in Figure 3 for the *z*- and *x*-axis, whereas excess, missing or overlapping material is represented as percentage of the corresponding targeted volume determined from the CAD file. As evident from Figure 3, the overlap of both matrices as well as the deficiency of material is more or less constant along the different axis of the scaffold. Exceptions are the outer boarders of the scaffold where material deficiency usually increases (not represented in Figure 3A) because the tiniest struts at the outside (see Figure 3B, cross sections z2, z3) break away easily during handling of the specimen. The analysis of the protruding material along the scaffolds individual axis on the other hand reveals strong variations, which represent the symmetric lattice shape with a repeating unit of half a unit cell. The scaffold features are repeated twice as much as the original repeating unit of 2 mm, because the rhombic cells are staggered by half unit cell width, as indicated in Figure 3, cross section x2. Each half unit, i. e. 1 mm, the amount of protruding material increases abruptly, independent of the scaffold axis. Nevertheless, the variation of the protruding material along the *z*-direction is higher, covering a range of 25 % to 140 %, than the variation along the *x*- and *y*-axis, which covers a range of 35 % to 120 %.

Reason for the variations in protruding material especially along the *z*-axis is the anisotropic SLM fabrication process. During the additive manufacturing process of SLM, subsequent layers of powder are selectively molten and solidified. Each melting process involves re-heating and re-melting of the already solidified material layers below and heat flux from the topmost layer to the bottom of the scaffold. This, for each layer repeated, process causes additional powder to adhere at the lower surface of struts and knots. Especially the lower surfaces of areas having small inclination angles with respect to the powder layer (*x*-*y*-plane) are susceptible for increased surface roughness [19] due to partly fused powder particles of different size. Also, stalactite formation at down facing faces decreases the surface quality [20]. Nevertheless, we find the highest percentage of protruding material exact in the middle of the knots where the struts merge (cp. Figure 2B, cross section z1, x1, x2). These peaks in protruding material correlate with the slices of the CAD file, which exhibit the lowest absolute volume (cp. Figure 2B, cross section z1). This minimum in absolute volume repeats after 1 mm because the unit cells are staggered by half unit cell width. The peaks of up to 140 % for protruding material are therefore caused by the data representation, which is relative to the targeted volume of the CAD file. Nevertheless, the main geometrical mismatch between CAD file und SLM-fabricated part is excess material at the down-facing surfaces caused by adhering powder particles and stalactite formation.

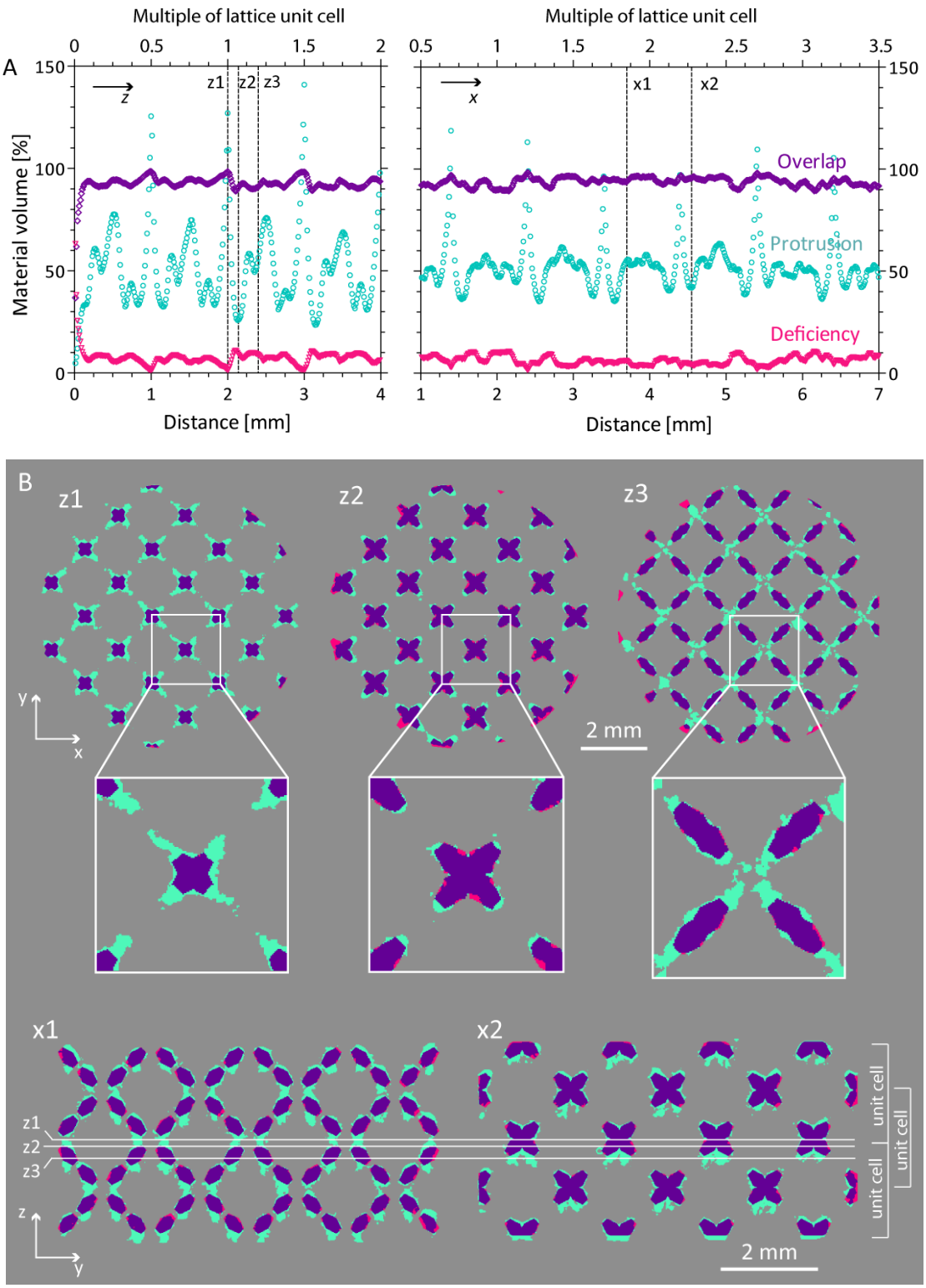

Figure 3. A: Volume of overlapping, protruding and deficient material in percentage of the target volume along the *z*- and the *x*-axis of the scaffold, respectively. B: Virtual cross sections as indicated in the graphs above along the *z*- and *x*-axis of the registered matrix, representing the overlapping (blue), protruding (light blue) and absent (pink) material.

Quality assessment for additive manufactured parts is usually done via investigations of closed porosity and surface roughness [21], both difficult to apply onto filigree and complex-shaped parts with inner structures inaccessible from the outside without specimen destruction. Therefore, the presented method of 3D data registration and analysis is a suitable tool for the quantification of the morphological quality of additive-manufactured scaffolds. Also, the method could be important for the optimization of process parameters, which play a major role for resulting properties in SLM-manufactured parts [5, 22].

3.2 Quantification of the one-way shape memory effect

To quantify the shape recovery of a pseudoplastically deformed SLM-built NiTi scaffold, seven out of the eleven datasets obtained from the continuous SRμCT measurement were registered with the CAD file as described above. The overall quantities for overlapping, protruding and deficient material depend on the temperature, as can be seen from the data summarized in Table 1. The quantities are represented relative to the CAD file, whereas the deviations were estimated to be ±0.6 % for the overlap, ±4.7 % for the protrusion and ±5.7 % for the deficiency.

Table 1. Overall quantities for overlap, protrusion and deficiency relative to the CAD file at different time and temperature points, respectively, before and during the shape recovery process.

	Dataset	Mean temperature	Overlap [%]	Protrusion [%]	Deficiency [%]
0	Prior to deformation	Ambient	92.55 ± 0.55	48.87 ± 2.30	7.45 ± 0.42
1	Deformed scaffold	18.0 °C	77.04 ± 0.46	69.89 ± 3.28	22.96 ± 1.31
2	↓	26.9 °C	79.51 ± 0.48	66.62 ± 3.13	20.49 ± 1.17
3		28.7 °C	82.51 ± 0.49	62.47 ± 2.94	17.49 ± 1.00
4	Shape recovery during heating	30.4 °C	87.70 ± 0.53	57.55 ± 2.70	12.30 ± 0.70
5		32.1 °C	91.08 ± 0.55	53.68 ± 2.52	8.92 ± 0.51
6	↓	32.9 °C	92.30 ± 0.55	51.06 ± 2.40	7.70 ± 0.44
7	Shape recovered	34.0 °C	92.36 ± 0.55	51.68 ± 2.42	7.64 ± 0.43

After completion of the shape recovery, the initial values of dataset #0 are almost entirely recovered. As evident from the data in Table 1, the shape recovery process is accomplished already in dataset #6, referring to a mean temperature of 32.9 °C. Even though each dataset was obtained over a temperature interval covering 3.0 to 4.5 K the evolution of the quantities for overlap, protrusion and deficiency with increasing temperature matches the progression of the scaffold height during temperature increase determined by a conventional TMA measurement, as exemplarily displayed for the quantity of overlapping material with temperature in Figure 4A. The thermoelectrically acquired temperature during the SRμCT measurement was corrected downwards by 7.5 K in accordance with the TMA investigations, which worked on a calibrated temperature sensor.

The temperature interval for the phase transformation from martensite to austenite measured with DSC at 10 K per minute differs from the temperature interval for the shape recovery observed via SRμCT, which has been conducted at a heating rate of 0.067 K per minute. The DSC revealed an A_f value of 41 °C, whereas we observed the fully recovered shape at 32.9 °C in the SRμCT experiment, meaning that the phase transformation is terminated at lower temperatures in the SRμCT investigation. The difference is caused by the distinct heating rates applied in the two experiments. Decreasing the heating rate results in decreased temperatures for the austenitic phase transformation whereas A_s is less heating rate sensitive than A_f [23, 24].

Figure 4B displays the progression of the overlapping material along the scaffolds *z*-axis for the datasets prior and subsequent to deformation as well as after the completed shape memory effect. The data clearly show the almost exact matching of the scaffolds shape prior to deformation and after conducted shape memory effect.

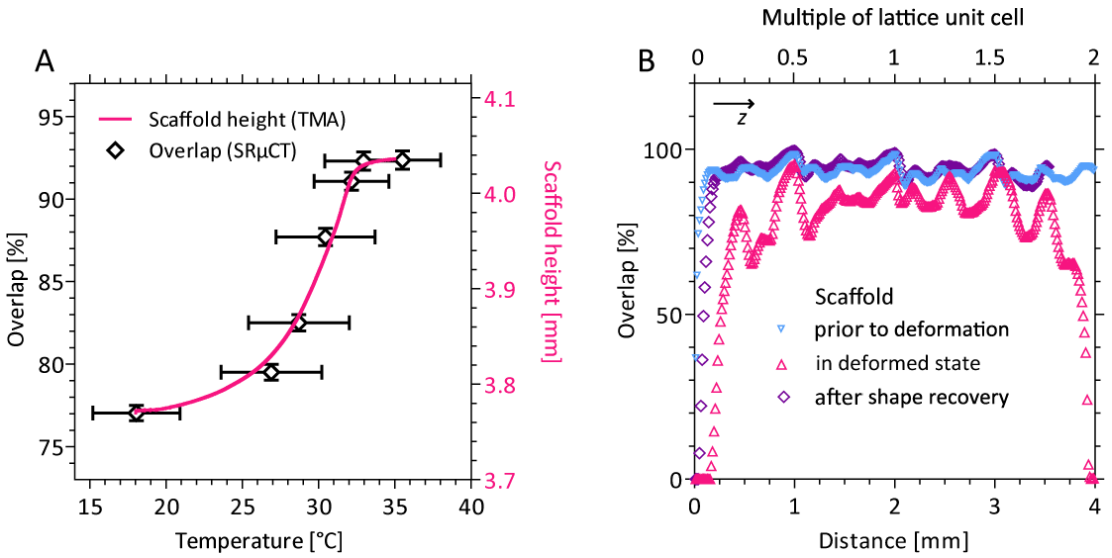

Figure 4A. Overall overlap of the initial file with the seven datasets reconstructed from the SRμCT data obtained during heating of the deformed scaffold and TMA curve of the deformed scaffold. The deviations for the temperature in the SRμCT measurements cover the temperature interval during data acquisition and the assumed measuring inaccuracy. B: Overlap along the *z*-axis for the non-deformed and deformed scaffold as well as the scaffold after completed shape recovery.

4. CONCLUSIONS

The morphology of parts fabricated by selective laser melting can be assessed and quantified by registration of SRμCT and CAD data. The evaluation of 3D data is in particular expedient for complex-shaped parts, whose porous structure cannot be analyzed without sectioning. Continuously acquired SRμCT data or radiograph recording has proven to be a suitable technique to analyze the temperature-dependent deformation of NiTi scaffolds. Even though the reconstructed datasets initially showed artifacts caused by slight movement of the specimen, we found that progression of the extracted quantities with time and temperature, respectively, agrees well with the progression of the macroscopic parameter scaffold height vs. temperature determined by conventional TMA measurements. The data will serve for the determination of local deformations within scaffolds and the evaluation of cell-response in presence of mechanical stimuli. Based on this approach, scaffold design and loading regime should be refined and optimized with respect to the actual physiological situation.

REFERENCES

[1] Bansiddhi, A., T.D. Sargeant, S.I. Stupp, and D.C. Dunand, "Porous NiTi for bone implants: a review," Acta Biomater. 4(4), 773-82 (2008).

[2] Liu, X., S. Wu, K.W.K. Yeung, Y.L. Chan, T. Hu, Z. Xu, X. Liu, J.C.Y. Chung, K.M.C. Cheung, and P.K. Chu, "Relationship between osseointegration and superelastic biomechanics in porous NiTi scaffolds," Biomaterials 32(2), 330-338 (2011).

[3] Rucci, N., "Molecular biology of bone remodelling," Clinical Cases in Mineral and Bone Metabolism 5(1), 49-56 (2008).

[4] Hill, P.A. and M. Orth, "Bone remodelling," J. Orthod. 25, 101-107 (1998).

[5] Bormann, T., R. Schumacher, B. Müller, M. Mertmann, and M. de Wild, "Tailoring selective laser melting process parameters for NiTi implants," J. Mater. Eng. Perform. 21(12), 2519-2524 (2012).

[6] Bormann, T., R. Schumacher, B. Müller, and M. de Wild, "From powder to complex-shaped NiTi structures by selective laser melting," Euro PM2012 Proceedings 1(Applications and New Processes), 193-197 (2012).

[7] Schulz, G., H.J.A. Crooijmans, M. Germann, K. Scheffler, M. Müller-Gerbl, and B. Müller, "Three-dimensional strain fields in human brain resulting from formalin fixation," J. Neurosci. Methods 202, 17-27 (2011).
[8] Frost, M., "A 2003 update of bone physiology and Wolff's law for clinicians," Angle Orthod. 74(1), 3-13 (2004).
[9] Yang, P.F., G.P. Brüggemann, and J. Rittweger, "What do we currently know from in vivo bone strain measurements in humans?," J. Musculoskelet. Neuronal Interact. 11(1), 8-20 (2011).
[10] Vandamme, K., I. Naert, J.V. Sloten, R. Puers, and J. Duyck, "Effect of implant surface roughness and loading on peri-implant bone formation," J. Periodont. 79(1), 150-157 (2008).
[11] Zhang, X., K. Vandamme, A. Torcasio, T. Ogawa, G.H. van Lenthe, I. Naert, and J. Duyck, "In vivo assessment of the effect of controlled high- and low-frequency mechanical loading on peri-implant bone healing," J. R. Soc. Interface 9(72), 1697-1704 (2012).
[12] Beckmann, F., J. Herzen, A. Haibel, B. Müller, and A. Schreyer, "High density resolution in synchrotron-radiation-based attenuation-contrast microtomography," Proc. of SPIE 7078, 70781D (2008).
[13] Müller, B., P. Thurner, F. Beckmann, T. Weitkamp, C. Rau, R. Bernhardt, E. Karamuk, L. Eckert, S. Buchloh, E. Wintermantel, D. Scharnweber, and H. Worch "Three-dimensional evaluation of biocompatible materials by microtomography using synchrotron radiation," Proc. of SPIE 4503, 178-188 (2002).
[14] Thurner, P.J., F. Beckmann, and B. Müller, "An optimization procedure for spatial and density resolution in hard X-ray micro-computed tomography," Nucl. Instrum. Methods Phys. Res. Sect. B-Beam Interact. Mater. Atoms 225, 99–603 (2004).
[15] Kak, A.C. and M. Slaney, *Principles of Computerized Tomographic Imaging*. 1988: IEEE Press.
[16] Müller, B., H. Deyhle, S. Lang, G. Schulz, T. Bormann, F. Fierz, and S. Hieber, "Three-dimensional registration of tomography data for quantification in biomaterials science," Int. J. Mater. Res. 103(2), 242-249 (2012).
[17] Andronache, A., M. von Siebenthal, G. Szekely, and P. Cattin, "Non-rigid registration of multi-modal images using both mutual information and cross-correlation," Med. Image Anal. 12, 3-15 (2008).
[18] Fierz, F.C., F. Beckmann, M. Huser, S.H. Irsen, B. Leukers, F. Witte, O. Degistirici, A. Andronache, M. Thie, and B. Muller, "The morphology of anisotropic 3D-printed hydroxyapatite scaffolds," Biomaterials 29(28), 3799-806 (2008).
[19] Strano, G., L. Hao, R.M. Everson, and K.E. Evans, "Surface roughness analysis in selective laser melting", in: Innovative Developments in Design and Manufacturing: Advanced Research in Virtual and Rapid Prototyping. 2012, CRC Press-Taylor & Francis Group: Boca Rano. p. 561-565.
[20] Vandenbroucke, B. and J.-P. Kruth, "Selective laser melting of biocompatible metals for rapid manufacturing of medical parts," Rapid Prototyping J. 13(4), 196-203 (2007).
[21] Bremen, S., W. Meiners, and A. Diatlov, "Selective laser melting: a manufacturing technology for the future?," Laser Technik Journal 2, 33-38 (2012).
[22] Kempen, K., E. Yasa, L. Thijs, J.-P. Kruth, and J. van Humbeeck, "Microstructure and mechanical properties of selective laser melted 18Ni-300 steel," Physics Procedia 12, 255-263 (2011).
[23] Nurveren, K., A. Akdogan, and W.M. Huang, "Evolution of transformation characteristics with heating/cooling rate in NiTi shape memory alloys," J. Mater. Process. Technol. 196, 129–134 (2008).
[24] Wang, Z.G., X.T. Zu, and Y. Huo, "Effect of heating/cooling rate on the transformation temperatures in TiNiCu shape memory alloy," Thermochim. Acta 436, 153–155 (2005).